Journal of Solid State Chemistry 183 (2010) 2365–2371

Contents lists available at ScienceDirect

Journal of Solid State Chemistry

journal homepage: www.elsevier.com/locate/jssc

Thermoluminescence and synchrotron radiation studies on the persistent luminescence of $BaAl_2O_4:Eu^{2+},Dy^{3+}$

L.C.V. Rodrigues [a,b], R. Stefani [a], H.F. Brito [a,*], M.C.F.C. Felinto [c], J. Hölsä [b,d], M. Lastusaari [b,d], T. Laamanen [b,e], M. Malkamäki [b,e]

[a] Universidade de São Paulo, Instituto de Química, Departamento de Química Fundamental, Av. Prof. Lineu Prestes, 748, CEP 05508-900, São Paulo, SP, Brazil
[b] University of Turku, Department of Chemistry, FI-20014 Turku, Finland
[c] Instituto de Pesquisas Energéticas e Nucleares, Centro de Química e Meio Ambiente, Av. Prof. Lineu Prestes, 2242, São Paulo, SP, Brazil
[d] Turku University Centre for Materials and Surfaces (MatSurf), Turku, Finland
[e] Graduate School of Materials Research (GSMR), Turku, Finland

ARTICLE INFO

Article history:
Received 25 May 2010
Received in revised form
22 July 2010
Accepted 27 July 2010
Available online 4 August 2010

Keywords:
Persistent luminescence
Barium aluminate
Europium
Thermoluminescence
Synchrotron radiation
DFT

ABSTRACT

The persistent luminescence materials, barium aluminates doped with Eu^{2+} and Dy^{3+} ($BaAl_2O_4:Eu^{2+},Dy^{3+}$), were prepared with the combustion synthesis at temperatures between 400 and 600 °C as well as with the solid state reaction at 1500 °C. The concentrations of Eu^{2+}/Dy^{3+} (in mol% of the Ba amount) ranged from 0.1/0.1 to 1.0/3.0. The electronic and defect energy level structures were studied with thermoluminescence (TL) and synchrotron radiation (SR) spectroscopies: UV–VUV excitation and emission, as well as with X-ray absorption near-edge structure (XANES) methods. Theoretical calculations using the density functional theory (DFT) were carried out in order to compare with the experimental data.

1. Introduction

Since 1995, the research on persistent luminescence materials has increased substantially [1,2]. This is due to the progress in the properties of these materials: they can emit nowadays in visible for many, up to 24+ h, after ceasing the irradiation. Because of the long emitting time, these phosphors can be exploited commercially in emergency signs, road signalization, wall painting, watches, microdefect sensing, optoelectronics for image storage and detectors of high energy radiation [3–6]. The persistent luminescence is not any more just a scientific curiosity.

Although the persistent luminescence from the Bologna Stone has been known for more than 400 years [1,2], only since the mid-1990s the truly useful and efficient persistent luminescent phosphors were developed and, to a certain extent, entered into the commercial market, too. These new phosphors originally included only the Eu^{2+} doped alkaline earth aluminates, $MAl_2O_4:Eu^{2+}$ (*M*: Ca, Sr and Ba) [1,7–12], but other, more complex aluminates, e.g. Eu^{2+} or Ce^{3+} doped melilite based aluminosilicates ($Ca_2Al_2SiO_7:Eu^{2+}$, $CaYAl_3O_7:Eu^{2+},Dy^{3+}$ [13–15], etc.) have been studied as well but gained no further interest because of their rather mediocre persistent luminescence properties.

At present, the Eu^{2+} doped alkaline earth aluminates remain, however, among the most important persistent phosphors, especially because their persistent luminescence can be greatly enhanced by co-doping with selected R^{3+} (R: rare earth) ions as Dy^{3+} and Nd^{3+}. The performance of the new aluminate based persistent luminescence phosphors is much superior to that of the conventional ZnS:Cu,Co material and they are visible to naked eye for more than 10 h in the dark after the exposure to irradiation [16]. Among these phosphors, the $BaAl_2O_4:Eu^{2+},R^{3+}$ materials have a special property that europium can be reduced without the use of a reducing atmosphere [17,18] that facilitates the preparation of these persistent luminescence materials.

There are plenty of mechanisms proposed for the persistent luminescence phenomenon [3,4,10,19,20]. The credibility of the mechanisms has evolved since the first ones in 1996, but even today there are still some contradictions between them. The most accepted mechanism considers that (i) under irradiation of the material some electrons escape from the $4f^65d^1$ levels of Eu^{2+} to the conduction band, (ii) some of these electrons are trapped from the conduction band to defects as oxygen vacancies, and possibly to the R^{3+} co-dopant, too and (iii) the reverse process of freeing the electrons from the traps to the $4f^65d^1$ levels of Eu^{2+} *via* the

* Corresponding author. Fax: +55 11 38155579.
E-mail address: hefbrito@iq.usp.br (H.F. Brito).

0022-4596/$ - see front matter © 2010 Elsevier Inc. All rights reserved.
doi:10.1016/j.jssc.2010.07.044

conduction band precedes the radiative relaxation of the electron back to the $4f^7$ ($^8S_{7/2}$) ground state of Eu^{2+} and the creation of the persistent luminescence [4]. However, the understanding of the detailed mechanism is still rather poor. Systematic studies of the persistent luminescence materials are necessary to achieve a better understanding of the relation between the materials' properties and their persistent luminescence [6].

According to the literature, the $BaAl_2O_4(:Eu^{2+},R^{3+})$ materials are prepared via a solid state route, usually by heating $BaCO_3$ with Al_2O_3 (or their precursors) at elevated temperatures. However, low temperature routes as combustion and sol–gel syntheses are not uncommon [21–26]. In the present work, the $BaAl_2O_4$:Eu^{2+},Dy^{3+} materials were prepared with different synthesis methods and with different Eu^{2+} and Dy^{3+} concentrations. The effect on the materials purity (and structure), trap structure, band gap energy and oxidation state of europium are presented and discussed based on the analysis of the X-ray powder diffraction (XRD), scanning electron microscopy (SEM), thermoluminescence (TL), synchrotron radiation (SR) UV–VUV spectroscopy and SR X-ray absorption results. The density functional theory (DFT) calculations were also carried out to determine the band gap energy of the non-doped $BaAl_2O_4$.

2. Materials and methods

2.1. Materials preparation

The $BaAl_2O_4$:Eu^{2+},Dy^{3+} materials were prepared with both the solid state and combustion reactions. For the solid state reaction, stoichiometric amounts of $Ba(NO_3)_2$, Al_2O_3, $Eu(NO_3)_3 \cdot 6H_2O$ and $Dy(NO_3)_3 \cdot 6H_2O$ were ground intimately. The mixtures were then heated in static air at 700 and 1500 °C for 2 and 5 h, respectively. The materials were doped and co-doped with the following nominal concentrations of Eu^{2+}/Dy^{3+} (in mol% of the Ba^{2+} amount):
0.1/0.1, 0.25/0.5, 0.5/0.5, 1.0/2.0 and 1.0/3.0.

For the combustion synthesis, the metal nitrates and urea were used as reactants and fuel, respectively. The precursors were dissolved into the smallest possible amount of distilled water. A silica capsule filled with the homogeneous solution was inserted into a furnace pre-heated at 400, 500 or 600 °C [24–26]. The reaction began after *ca.* 5 min after the introduction of the capsule into the furnace. The mixture was then self-ignited with a white flame and produced a white powder. In this chemical reaction, H_2O, NH_3, CO_2, O_2 and N_2 gases are released though the reactions are complex and are not known in detail. After the completion of the reaction, the furnace was turned off and was left to cool freely. The products were removed from the furnace when the temperature had decreased to *ca.* 25 °C. The nominal concentrations of Eu^{2+} and Dy^{3+} (in mol% of the Ba^{2+} amount) were 1.0 and 2.0, respectively. The europium and dysprosium nitrates were obtained from the respective oxides with a reaction with concentrated nitric acid.

2.2. X-ray powder diffraction

The crystal structure and phase purity of the $BaAl_2O_4$:Eu^{2+},Dy^{3+} materials were verified with the X-ray powder diffraction measurements. The XRD patterns were recorded with a Huber G670 image plate (2θ range: 4–100°, step: 0.005°) Guinier camera ($CuK\alpha_1$ radiation at 1.5406 Å).

The average crystal size of the materials was estimated from the diffraction data by using the Scherrer formula (Eq. 1) [27] where D is the average crystal size (m), λ the X-ray wavelength (m), β the full width at half maximum (FWHM) of the selected reflection (rad) and θ (°) half of the Bragg angle (2θ). In the present work, [202] reflection (2θ: 28.3°) was used in the calculations. The reflection broadening due to the diffractometer setup was eliminated from the β_s value (Eq. 2) by using a microcrystalline silicon (Si) reference (β_R). It should be realized that the Scherrer equation can be applied only to materials with an average crystal size of less than *ca.* 200 nm [27].

$$D = \frac{0.9\,\lambda}{\beta \cos\theta} \tag{1}$$

$$\beta^2 = \beta_s^2 - \beta_r^2 \tag{2}$$

2.3. Scanning electron microscopy (SEM)

The electron microscopic analysis of the $BaAl_2O_4$:Eu^{2+},Dy^{3+} materials prepared with the solid state and combustion methods was carried out with a JEOL JSM-740 1F Field Emission Scanning Electron Microscope.

2.4. Synchrotron radiation UV–VUV spectroscopy

The SR excitation and emission spectra of the $BaAl_2O_4$:Eu^{2+} materials were measured between 80 and 330 as well as 200 and 620 nm, respectively, by using the UV–VUV synchrotron radiation facility at the SUPERLUMI beam line of HASYLAB at DESY (Hamburg, Germany) [28]. The samples were mounted on the cold finger of a liquid He flow cryostat and the spectra were recorded at selected temperatures between 10 and 298 K. The setup consisted of a 2-m McPherson primary monochromator with a resolution up to 0.02 nm (excitation) and an ARC SpectraPro-308i monochromator equipped with a Hamamatsu R6358P photomultiplier (emission). The UV–VUV excitation spectra were corrected for the incident flux of the excitation beam using the excitation spectrum of sodium salicylate as a standard.

2.5. X-ray absorption measurements

The X-ray absorption near-edge structure (XANES) spectroscopy measurements of europium in the $BaAl_2O_4$:Eu^{2+},Dy^{3+} persistent luminescence materials prepared with different methods were measured at room temperature using the beamline I811 at MAX-lab in Lund, Sweden [29]. The freshly annealed europium oxide (Eu_2O_3) was measured as the reference. The data were collected in the fluorescence mode at room temperature over the Eu L_{III} edge using the Si(111) double crystal monochromator with a 7 element Gresham Si(Li) detector. The energy resolution $\Delta E/E$ was 10^{-4} and the measured energy range was 100 eV both before and after the edge.

2.6. Thermoluminescence

The TL glow curves of the $BaAl_2O_4$:Eu^{2+},Dy^{3+} phosphors were recorded with an upgraded Risø TL/OSL-DA-12 thermoluminescence system with a linear heating rate of 5 °C s^{-1} in the temperature range between 25 and 400 °C. The global TL emission from UV to 650 nm was monitored. Prior to the TL measurements, the materials were exposed to radiation from a combination of the Philips TL 20W/05 (emission maximum at 360 nm) and 4W EW-098 17-20 (254 and 365 nm) UV lamps. Exposure times varied from 15 s to 30 min. The analysis of the TL glow curves was carried out by deconvoluting the TL curves with the program TLanal v1.0.3 [30,31], which uses the general approximation (GA)

method as a background. The fitted peaks were considered to be of the 1st or 2nd order kinetics depending on the peak shape.

2.7. Density functional theory calculations

The electronic band structure of the $BaAl_2O_4$ host was calculated using the WIEN2k package [32]. WIEN2k is based on the full potential linearized augmented plane wave method, an approach that is among the most precise and reliable ways to calculate the electronic structure of solids. The generalized gradient approximation (GGA) was employed.

3. Results and discussion

3.1. Formation and phase purity of $BaAl_2O_4:Eu^{2+},Dy^{3+}$

Although the stoichiometric $BaAl_2O_4$ system shows complex polymorphism as a function of temperature [33,34], the XRD patterns for the $BaAl_2O_4$ materials with different (co-)dopant concentrations confirmed that the materials studied at room temperature were of the hexagonal $BaAl_2O_4$ form with the space group $P6_3$ [35]. However, $BaAl_{12}O_{19}$ was frequently observed as an impurity (Fig. 1) which is quite expected because the preparation of a similar material $BaAl_{10}O_{17}$ has been reported to proceed *via* the intermediate product of $BaAl_2O_4$ [36]. During the combustion synthesis, the temperature of the reaction mixture can achieve locally and for short periods of time rather high values, up to at least 1600 °C [37] (even higher temperatures as 3000 °C—depending on the fuel and oxidizer, of course, have been suggested). The local temperature may clearly reach to the temperature range of the formation of $BaAl_{10}O_{17}$, 1600–1800 °C [36] and exceed that of $BaAl_2O_4$, less than 1300 °C. An estimate for the amount of the $BaAl_{12}O_{19}$ impurity does not exceed 5% of the total material. No significant differences were observed in the 2θ position or FWHM of the XRD reflections between different materials. This is an indication of the low amount of (co-)dopants incapable to create stresses or strains in the $BaAl_2O_4$ lattice. On the other hand, the patterns showed the broadening of the reflections for the materials prepared with the combustion method. This broadening indicates a small crystallite size (Table 1) that can be calculated using the Scherrer formula given above.

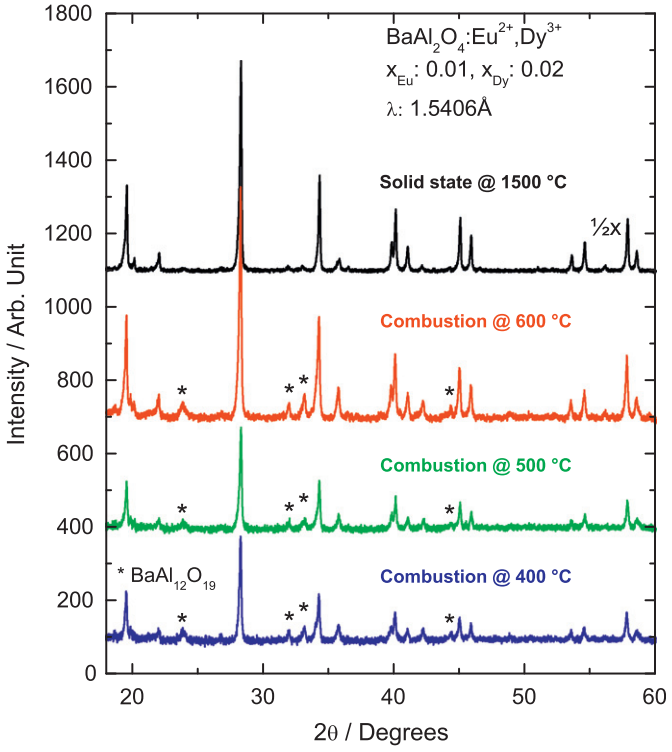

Fig. 1. X-ray powder diffraction patterns of the $BaAl_2O_4:Eu^{2+},Dy^{3+}$ phosphors prepared with different methods.

The large crystallite size (> 200 nm) of the solid state prepared material is due to the sintering occurring at the high temperatures used (1500 °C) though this value may be an underestimate since the Scherrer method is not suitable for the characterization of large crystal sizes [27]. For the materials prepared with the combustion synthesis, the crystallite size decreases from 98 to 85 nm with the increase in reaction temperature from 400 to 600 °C. This decrease is due to the fact that, at higher temperatures, the combustion reactions are faster and thus increase the local reaction temperature to even higher than at lower temperatures.

The SEM images of the $BaAl_2O_4:Eu^{2+},Dy^{3+}$ materials prepared with the solid state and combustion methods (Fig. 2) clearly show the large crystal size (*ca.* 3 μm) of the material prepared with the solid state method (Fig. 2a). This proved the unfeasibility of the Scherrer method to the characterization of large crystal sizes. In contrast, the SEM image of the combustion prepared material (Fig. 2b) indicates a small crystals size (*ca.* 90 nm), thus validating the crystal size calculated with the Scherrer method.

3.2. Trap depths

The persistent luminescence involves the release of electrons from traps with thermal energy. The most suitable method to observe the trap energies and densities is consequently the thermoluminescence spectroscopy though the nature of the traps is not easily obtained, nevertheless. The TL glow curves of the $BaAl_2O_4:Eu^{2+},Dy^{3+}$ materials prepared with the solid state method show a band of high intensity at *ca.* 70 °C with weaker bands at 120 and 200 °C (Fig. 3). These bands can be ascribed to the presence of either electron or hole traps (or both) in the energy gap of the host. These rather shallow traps are responsible for storing the energy for a short period of time only, i.e. they are responsible for the persistent luminescence in contrast to deep traps leading to the photostimulated luminescence. As a function of the (co-)dopant concentrations, the total TL intensity increases with the increase in Eu^{2+} and Dy^{3+} concentrations. This is consistent with the increase in the number of traps, especially with the increase in the Dy^{3+} concentration. The increase in the TL intensity with the increase in the Eu^{2+} concentration is due to the increase in the number of the emitting centers and certainly also to the increase in the probability of energy transfer from the traps to the emitting centers which are getting closer when the dopant concentration is increased.

Table 1
Effect of the preparation method of the $BaAl_2O_4:Eu^{2+},Dy^{3+}$ materials on the crystallite size, TL peak maximum and TL FWHM.

Method (°C)	Crystallite size (nm)	Thermoluminescence	
		Peak max (°C)	FWHM (°C)
Solid state at 1500	> 200 (*ca.* 3 μm from SEM)	68	32
Combustion at 400	98	73	38
Combustion at 500	82	76	44
Combustion at 600	85	76	44

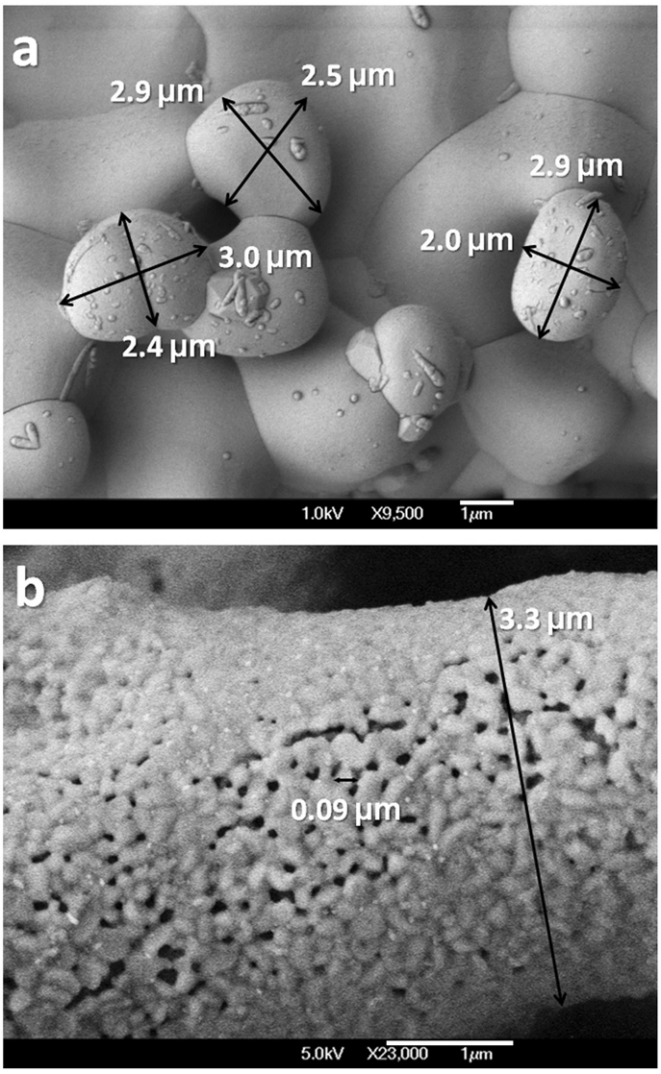

Fig. 2. SEM images of the $BaAl_2O_4:Eu^{2+},Dy^{3+}$ phosphors prepared with (a) the solid state method and (b) the combustion method.

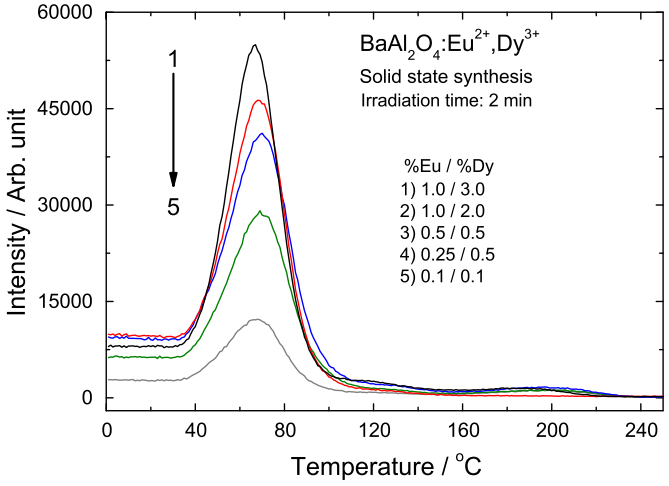

Fig. 3. TL glow curves of the $BaAl_2O_4:Eu^{2+},Dy^{3+}$ phosphors with different (co-)dopant concentrations.

The TL glow curves recorded for the $BaAl_2O_4:Eu^{2+},Dy^{3+}$ materials prepared with the combustion method (Fig. 4) show only one band centered at *ca.* 75 °C. The maximum intensity for this TL band was obtained for the material prepared at 500 °C which evolution cannot be explained at present. The position of the main band is very similar irrespective of the preparation method which suggests that the trap responsible for this band is very similar, too. There are some differences, nevertheless, the FWHM of the TL bands of the combustion method materials is much larger than that of the material prepared with the solid state method. In addition, the FWHM (Table 1) increases with the decrease in the crystallite size. These trends are due to a decrease in the heat transfer between the individual crystals with decreasing crystal size, which can induce a delay in the release of electrons from traps and broaden the TL bands. It should be noted that the heating rate is rather high, 5 °C s^{-1}. The other difference observed between the thermoluminescence glow curves of the solid state (Fig. 3) and the combustion (Fig. 4) prepared materials is the absence of the bands at 120 and 200 °C in the latter. The absence of these deep traps can be due to the short reaction time in the combustion synthesis (few seconds) when compared to the solid state syntheses (5 h). With this shorter reaction time, it is more difficult for the higher energy traps to achieve equilibrium. The $BaAl_{12}O_{19}$ impurity cannot be responsible for the absence of the weak TL bands since the impurities can create, not annihilate the TL bands.

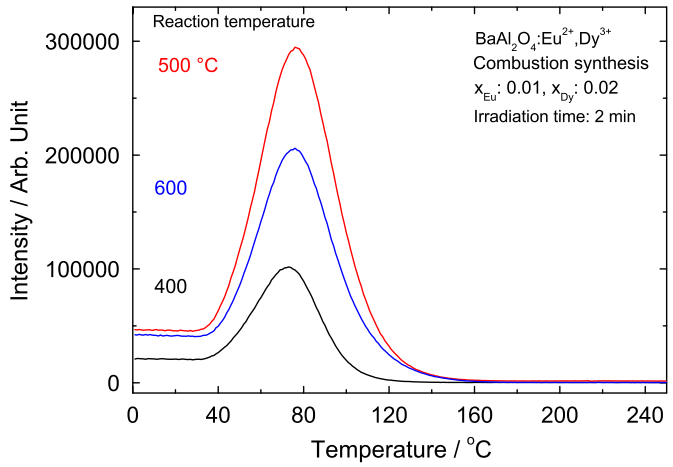

Fig. 4. TL glow curves of the $BaAl_2O_4:Eu^{2+},Dy^{3+}$ phosphors prepared with the combustion synthesis at 400, 500 and 600 °C.

In order to evaluate in a quantitative manner the effect of the dopant and co-dopant concentrations and the preparation method on the trap depths, the analysis of the TL curves was carried out by using the deconvolution of the glow curves [30,31]. The presence of three traps was confirmed for the material prepared with the solid state method (Fig. 5). The energy difference between the shallowest and the deeper traps was *ca.* 0.5 eV suggesting that efficient retrapping can occur. This is confirmed by the symmetric shape of the TL bands. The glow curves for the $BaAl_2O_4:Eu^{2+},Dy^{3+}$ materials prepared with the combustion method indicated the presence of only one trap, however. In agreement with the good persistent luminescence performance of all $BaAl_2O_4:Eu^{2+},Dy^{3+}$ materials studied, the energy of the shallowest trap did not vary much with the different (co-)dopant concentration or the preparation method.

3.3. SR excited luminescence of $BaAl_2O_4:Eu^{2+}$

The luminescence spectrum of the $BaAl_2O_4:Eu^{2+}$ material excited to the conduction band at 170 nm by synchrotron radiation (SR) is characterized by a high intensity band centered at *ca.* 505 nm (19800 cm^{-1}) with a FWHM value of 2200 cm^{-1}

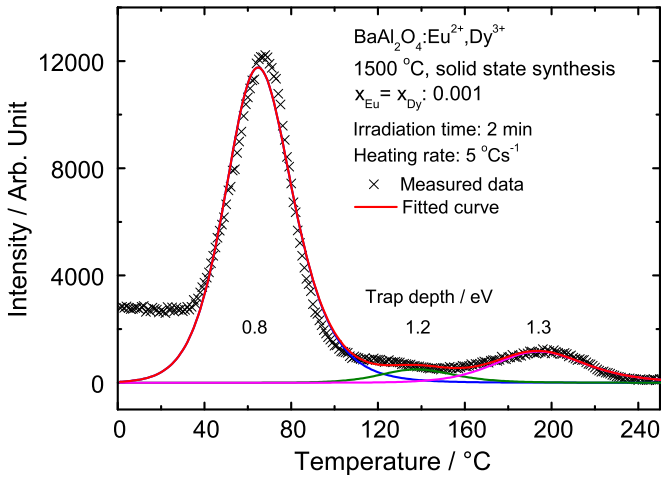

Fig. 5. Deconvolution of the TL glow curve for the $BaAl_2O_4:Eu^{2+},Dy^{3+}$ phosphor prepared with the solid state method at 1500 °C.

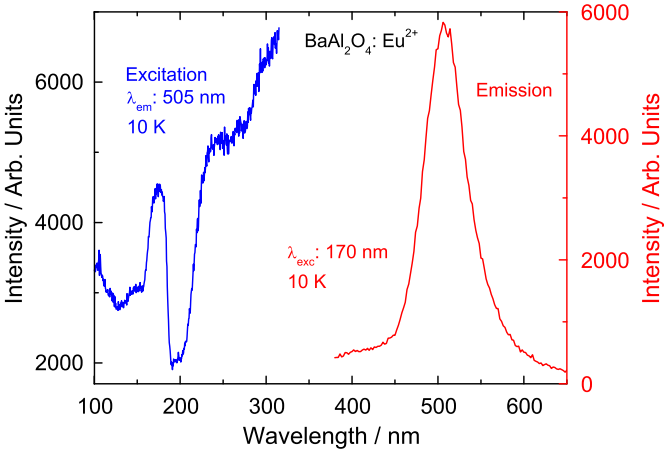

Fig. 6. Synchrotron radiation excited visible emission and UV–VUV excitation spectra of the Eu^{2+} doped $BaAl_2O_4$ at 10 K.

(Fig. 6). In the structure of $BaAl_2O_4$, there are two different barium sites, Ba(1) and Ba(2) though both are coordinated to nine oxygen atoms with slightly average Ba–O distances, 2.97 and 2.89 Å for Ba(1) and Ba(2), respectively [18]. However, the sharpness of the band is consistent with only one Ba^{2+} site occupied by Eu^{2+} ion in the $BaAl_2O_4$ lattice [35]. Despite the larger size of Ba^{2+}, no broadening of the Eu^{2+} emission band takes place due to a possible off-center position of Eu^{2+}. The single and symmetric band can thus be attributed to the straightforward $4f^65d^1 \rightarrow 4f^7$ transition of Eu^{2+} ion [38]. The other, much weaker band at *ca.* 440 nm may be due to the Eu^{2+} residing in the other Ba site. It is generally assumed that the persistent luminescence, and especially the storage of the excitation energy, is due to the presence of defects in the $BaAl_2O_4$ matrix. These defects may originate, due to high temperature synthesis, from the evaporation of BaO, which creates barium and oxide vacancies [5]. The presence of defects cannot, however, be detected as defect related luminescence or broadening and/or asymmetry of the Eu^{2+} emission band from $BaAl_2O_4:Eu^{2+}$. The defect related luminescence is probably absent as a result of efficient energy transfer from the defects to Eu^{2+} and the defect to Eu^{2+} distance may be long enough not to have a significant effect on the crystal field experienced by Eu^{2+} ion.

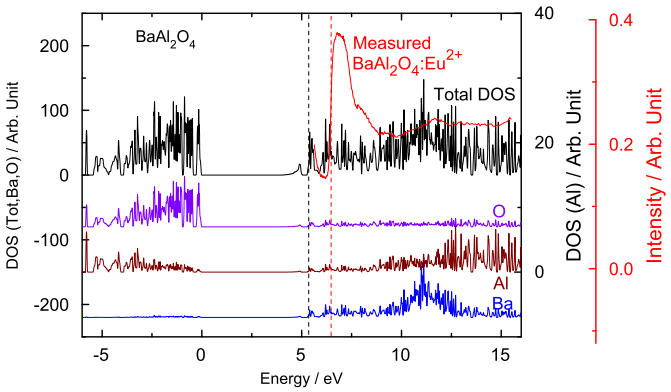

Fig. 7. Calculated density of states (DOS) for the $BaAl_2O_4$ host material with the DFT (GGA) method. Comparison is made with the UV–VUV excitation spectrum of $BaAl_2O_4:Eu^{2+}$ at 10 K.

3.4. SR excitation of $BaAl_2O_4:Eu^{2+}$

The SR excitation spectrum of the Eu^{2+} doped $BaAl_2O_4$ (Fig. 6) was recorded at 10 K to avoid the persistent luminescence that may smooth down the whole excitation spectrum, especially at room temperature. In the excitation spectrum, the broad bands between 210 (47600 cm^{-1}) and 334 nm (30000 cm^{-1}), the experimental limit of the setup, can be assigned to the $4f^7 \rightarrow 4f^65d^1$ transitions of the Eu^{2+} ion. These bands are composed of several overlapping bands corresponding to the splitting of the ^2D level of the $4f^65d^1$ configuration. In principle, each one of the individual broad bands should be composed of 7 sharper bands [39] due to the coupling of the $5d^1$ configuration with the ^7F_J (J: 0–6) components of $4f^6$ but, for the Eu^{2+} doped $BaAl_2O_4$, this fine structure cannot be observed due to e.g. severe overlap.

In addition to the interconfigurational $4f^7 \rightarrow 4f^65d^1$ transitions of Eu^{2+}, one can also observe a sharp edge at *ca.* 190 nm (6.5 eV). The edge is the fundamental absorption edge excitation corresponding, at least approximately, to the energy between the top of the valence band (VB) and the bottom of the conduction band (CB), i.e. the band gap energy, E_g. For a better estimate of E_g, the first derivate of the curve was plotted and the minimum gave the exact E_g value 52099 cm^{-1} (6.47 eV) for $BaAl_2O_4:Eu^{2+}$. This value, however, may be slightly too low since the possible excitonic fine structure [40] close to the bottom of the conduction band is not visible. The band gap energy of the non-doped material should be remeasured though, even then, it is not evident that this fine structure could be observed. Further speculation about the band gap and excitons seems futile at the moment though they could be of importance to the persistent luminescence and the trap energies.

3.5. Electronic band structure of $BaAl_2O_4$ by DFT calculations

The DFT calculations have been able to reproduce, in a surprisingly good agreement with experiment, the band gap energy as well as the position of the Eu^{2+} $^8S_{7/2}$ ($4f^7$) ground level position in the band gap for the $Sr_2MgSi_2O_7:Eu^{2+}$ persistent luminescence material [41]. Similar calculations for the $BaAl_2O_4$ host employing the GGA method (Fig. 7) presented a E_g value of 5.3 eV, which is a significantly lower value than the experimental one (6.5 eV). Taken into account the possible exciton contribution, the discrepancy may be even larger. The large difference between the calculated and experimental values is probably due to the higher than expected covalent character of bonding in $BaAl_2O_4$. The reasons for this discrepancy will be studied in detail in the future.

According to the DFT calculations, the valence band has mainly the O(2*p*) character while the bottom of the conduction band mostly consists of the Ba states. An oxygen or barium vacancy should thus create trapping sites for electrons or holes close to the bottom of CB or the top of VB, respectively. Most of the aluminum density of state (DOS) is located deep in the conduction band and should not be contributing to the formation of electron or hole traps. On the other hand, the creation of Al vacancies would demand high energies and is thus improbable.

3.6. Valence state of europium in $BaAl_2O_4$

It may generally be assumed that the aluminate based persistent luminescence materials are virtually free from trivalent europium due to the low europium concentration, lack of trivalent host cation of sufficiently large size and, of course, provided that the preparation usually with reducing gas sphere has been successful. If one or several of these conditions are not fulfilled, there might, indeed, be Eu^{3+} present in the materials. In most cases, probing of Eu^{3+} is not successful with the conventional luminescence techniques. An alternative, though quite expensive method is the XANES spectroscopy which was applied to the $BaAl_2O_4$:Eu^{2+},Dy^{3+} phosphors in this work, too. The XANES results indicate the co-existence of both the di- and trivalent europium for the materials made with both preparation methods (Fig. 8). However, it was observed that the trivalent form is by far the more dominant one. This predominance may be due to several factors that can occur simultaneously. First, during the preparation, the reduction of Eu^{3+} is not complete—with or without a reducing atmosphere. Second, in the proposed mechanism for persistent luminescence [2], the creation of a Eu^{2+}–h^+ (hole) pair or Eu^{3+} is compulsory as a result of the escape of the electron from Eu^{2+} to the conduction band during the charging step of persistent luminescence. Finally, the oxidation of Eu^{2+} by the X-rays should be considered. The first choice can be ruled out, since the sharp lines attributed to the intraconfigurational $4f^7$ transitions of Eu^{3+} were not observed either in the SR (Fig. 6) or UV excited emission spectra [17]. Even with excitation at 393 nm, region of the $^7F_0 \rightarrow {}^5L_6$ transition of Eu^{3+}, it is not possible to observe the $^5D_0 \rightarrow {}^7F_2$ hypersensitive transition of Eu^{3+} (Supporting Information Fig. S1). If Eu^{3+} is present, the absence of the 4f-4f transitions of Eu^{3+} may be due to non-radiative processes (quenching) by Eu^{2+} whose $4f^65d^1 \rightarrow 4f^7$ transitions are allowed, having a much shorter lifetime (*ca.* 1 μs) than the $4f \rightarrow 4f$ transitions of Eu^{3+} (several ms) and thus larger transition probability.

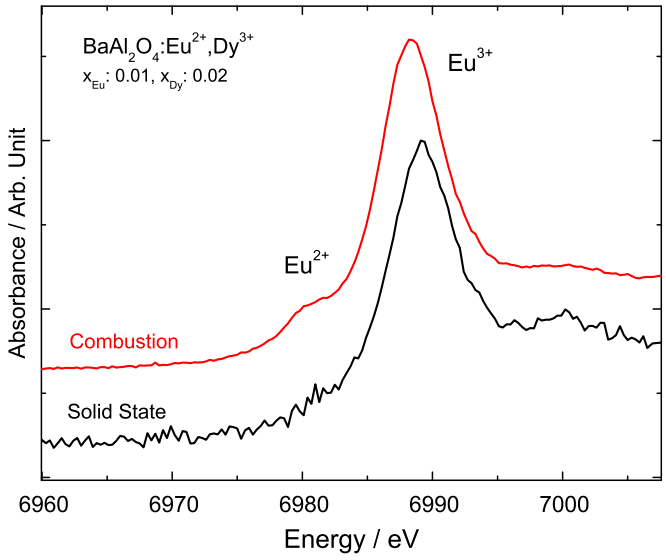

Fig. 8. Eu (L_{III}) XANES spectra of the $BaAl_2O_4$:Eu^{2+},Dy^{3+} phosphors prepared with the solid state and combustion methods.

The formation of Eu^{2+} using Eu^{3+} as a source without the use of reductive atmosphere can be explained by the evaporation of interstitial oxygen at high temperatures, similar to the evaporation that takes place in high-T_c cuprate superconductors. The probable mechanism for this reduction is shown by Eqs. (3)–(5). In this presentation, the Kröger–Vink notation [42] is used allowing the easy understanding of the species capable of trapping electrons and holes. All the symbols have their usual meanings except for the *relative* charges marked as follows: • (positive), ′ (negative) and $^\times$ (zero charge). Despite the simplicity of the Kröger–Vink notations, one can find quite a confusion about the use and definition of these notations [18]:

$$2Eu^{3+} + 3O^{2-} \rightarrow 2Eu^{\bullet}_{Ba} + 2O^{\times}_{O} + O''_i \quad (3)$$

$$2O''_i \rightarrow O_2(g) + 4e' \quad (4)$$

$$2Eu^{\bullet}_{Ba} + 2e' \rightarrow 2Eu^{\times}_{Ba} \quad (5)$$

The presence of Eu^{3+} is thus due to either the oxidation by X-rays or to the persistent luminescence mechanism. The former process should be irreversible whereas the latter is reversible and thus they should be easy to make a difference. Further work is in progress to clarify this matter.

4. Conclusions

The $BaAl_2O_4$:Eu^{2+},Dy^{3+} materials were prepared with both solid state and combustion syntheses. As usual, the combustion synthesis produces crystals with smaller size, evidently due to higher local temperature during the spontaneous explosion. Since the thermoluminescence analyses suggested the presence of one and three traps for the combustion and solid state prepared materials, respectively, the method of preparation has a significant effect on the defect structure of the materials. The mismatch between the band gap (E_g) value obtained from the synchrotron radiation excitation spectra and the DFT calculation was deduced to result from the covalent bonding in the $BaAl_2O_4$ host. The XANES spectroscopy showed a predominance of Eu^{3+} which can be present as a result of the *in situ* conditions of persistent luminescence during the X-ray irradiation. A systematic study of the effect of other R^{3+} co-dopants than Dy^{3+} is needed for a better understanding of the persistent luminescence mechanism of $BaAl_2O_4$:Eu^{2+},Dy^{3+}.

Acknowledgments

The authors thank Conselho Nacional de Desenvolvimento Científico e Tecnológico (CNPq), Fundação de Amparo à Pesquisa do Estado de São Paulo (FAPESP), Rede de Nanotecnologia Molecular e de Interfaces (RENAMI), Instituto do Milênio de Materiais Complexos (IM2C), Instituto Nacional de Ciência e Tecnologia—Nanotecnologia para Marcadores Integrados (inct-INAMI) and Coimbra Group for financial support to the Brazilian authors. The Finnish authors thank for the financial support from the Turku University Foundation, Jenny and Antti Wihuri Foundation (Finland) and the Academy of Finland. The synchrotron radiation study (HASYLAB, Germany) was supported by the European Community—Research Infrastructure Action under the FP6 Structuring the European Research Area Program, RII3-CT-2004-506008 (IA-SFS). Dr. Aleksei Kotlov (HASYLAB), as well as Dr. Stefan Carlson and Dr. Katarina Norén (MAX-lab) are gratefully acknowledged for their assistance during the synchro-

tron measurements. The DFT study was supported by research mobility agreements (112816/2006/JH and 116142/2006/JH, 123976/2007/TL) between the Academy of Finland and the Academy of Sciences of the Czech Republic. The DFT calculations were carried out using the supercomputing resources of the CSC IT Center for Science (Espoo, Finland) and in co-operation with Dr. P. Novák (Academy of Sciences of the Czech Republic). Dr. J. Niittykoski, Prof. K.O. Eskola and Prof. H. Jungner (University of Helsinki, Finland) are thanked for the measurement of the thermoluminescence glow curves.

Appendix A. Supplementary material

Supplementary data associated with this article can be found in the online version at doi:10.1016/j.jscc.2010.07.044.

References

[1] E. Newton Harvey, A history of luminescence: from the earliest times until 1900, Am. Philos. Soc. Philadelphia (1957) 305.
[2] J. Hölsä, Electrochem. Soc. Interface 18 (4) (2009) 42–45.
[3] T. Matsuzawa, Y. Aoki, M. Takeuchi, Y. Murayama, J. Electrochem. Soc. 143 (1996) 2670–2673.
[4] T. Aitasalo, J. Hölsä, H. Jungner, M. Lastusaari, J. Niittykoski, J. Phys. Chem. B 110 (2006) 4589–4598.
[5] J. Trojan-Piegza, J. Niittykoski, J. Hölsä, E. Zych, Chem. Mater. 20 (2008) 2252–2261.
[6] J. Hölsä, T. Laamanen, M. Lastusaari, M. Malkamäki, P. Novák, J. Lumin. 129 (2009) 1606–1609.
[7] W.Y. Jia, H.B. Yuan, L.Z. Lu, H.M. Liu, W.M. Yen, J. Cryst. Growth 200 (1999) 179–184.
[8] J. Hölsä, T. Laamanen, M. Lastusaari, M. Malkamäki, J. Niittykoski, P. Novák, Radiat. Phys. Chem. 78 (2009) 11–16.
[9] J. Hassinen, J. Hölsä, J. Niittykoski, T. Laamanen, M. Lastusaari, M. Malkamäki, P. Novák, Opt. Mater. 31 (2009) 1751–1754.
[10] F. Clabau, X. Rocquefelte, T. Le Mercier, P. Deniard, S. Jobic, M.H. Whangbo, Chem. Mater. 18 (2006) 3212–3220.
[11] X.D. Lu, W.G. Shu, Q. Fang, Q.M. Yu, X.Q. Xiong, J. Mater. Sci. 42 (2007) 6240–6245.
[12] T. Katsumata, R. Sakai, S. Komuro, T. Morikawa, H. Kimura, J. Cryst. Growth 198 (1999) 869–871.
[13] R. Sakai, T. Katsumata, S. Komuro, T. Morikawa, J. Lumin. 85 (1999) 149–154.
[14] M. Yamaga, Y. Ohsumi, T. Nakayama, N. Kashiwagura, N. Kodama, T.P.J. Han, J. Mater. Sci. Mater. Electron. 20 (2009) 471–475.
[15] N. Kodama, Y. Tanii, M. Yamaga, J. Lumin. 87-89 (2000) 1076–1078.
[16] T. Aitasalo, P. Dereń, J. Hölsä, H. Jungner, J.-C. Krupa, M. Lastusaari, J. Legendziewicz, J. Niittykoski, W. Strȩk, J. Solid State Chem. 171 (2003) 114–122.
[17] R. Stefani, L.C.V. Rodrigues, C.A.A. Carvalho, M.C.F.C. Felinto, H.F. Brito, M. Lastusaari, J. Hölsä, Opt. Mater. 31 (2009) 1815–1818.
[18] M. Peng, G. Hong, J. Lumin. 127 (2007) 735–740.
[19] P. Dorenbos, J. Electrochem. Soc. 152 (2005) H107–H110.
[20] T. Aitasalo, J. Hölsä, H. Jungner, M. Lastusaari, J. Niittykoski, J. Lumin. 94 (2001) 59–63.
[21] C.A. Zhang, L. Wang, L.P. Cui, Y.F. Zhu, J. Cryst. Growth 255 (2003) 317–323.
[22] G.M. Qiu, Y.J. Chen, X.J. Geng, L.J. Xiao, Y.G. Tian, Y.B. Sun, J. Rare Earths 23 (2005) 629–632.
[23] H. Aizawa, S. Komuro, I. Katsumata, S. Sato, T. Morikawa, Thin Solid Films 496 (2006) 179–182.
[24] Z. Qiu, Y. Zhou, M. Lu, A. Zhang, Q. Ma, Acta Mater. 55 (2007) 2615–2620.
[25] S. Ekambaram, K.C. Patil, M. Maaza, J. Alloys Compd. 393 (2005) 81–92.
[26] B.M. Mothudi, O.M. Ntwaeaborwa, J.R. Botha, H.C. Swart, Physica B 404 (2009) 4440–4444.
[27] H.P. Klug, L.E. Alexander, in: X-ray Powder Diffraction Procedures, Wiley, New York, 1959.
[28] 〈http://hasylab.desy.de/facilities/doris_iii/beamlines/i_superlumi〉 (accessed in 05/18/2010).
[29] 〈www.maxlab.lu.se/beamlines/bli811〉 (accessed in 05/18/2010).
[30] K.S. Chung, H.S. Choe, J.I. Lee, J.L. Kim, S.Y. Chang, Radiat. Prot. Dosim. 115 (2005) 345–349.
[31] K.S. Chung, TL Glow Curve Analyzer v.1.0.3., Korea Atomic Energy Research Institute and Gyeongsang National University, Korea, 2008.
[32] P. Blaha, K. Schwarz, G.K.H. Madsen, G. Kvasnicka, J. Luitz, in: K. Schwarz (Ed.), WIEN2k: An Augmented Plane Wave + Local Orbitals Program for Calculating Crystal Properties, Vienna University of Technology, Vienna, 2001.
[33] Q.L. Wu, Z. Liu, H. Jiao, Physica B 404 (2009) 2499–2502.
[34] J.M. Perez-Mato, R.L. Withers, A.K. Larsson, D. Orobengoa, Phys. Rev. B 79 (2009) 064111.
[35] S.Y. Huang, R. von der Mühll, J. Ravez, J.P. Chaminade, P. Hagenmuller, M. Couzi, J. Solid State Chem. 109 (1994) 97–105.
[36] S. Oshio, K. Kitamura, T. Shigeta, S. Horii, T. Matsuoka, S. Tanaka, H. Kobayashi, J. Electrochem. Soc. 146 (1999) 392–399.
[37] H.S. Jeon, S.K. Kim, H.L. Park, G.C. Kim, J.H. Bang, M. Lee, Solid State Commun. 120 (2001) 221–225.
[38] S.H.M. Poort, W.P. Blokpoel, G. Blasse, Chem. Mater. 7 (1995) 1547–1551.
[39] J.E. Van Haecke, P.F. Smet, D. Poelman, J. Lumin. 126 (2007) 508–514.
[40] P. Dorenbos, Phys. Status Solidi b 242 (2005) R7–R9.
[41] J. Hölsä, M. Kirm, T. Laamanen, M. Lastusaari, J. Niittykoski, P. Novák, J. Lumin. 129 (2009) 1560–1563.
[42] F.A. Kröger, H.H. Vink, in: Relations Between the Concentrations of Imperfections in Crystalline Solids in Solid State Physics, Academic Press, San Diego, 1995.